Journal of Radiation Research, Vol. 59, No. 2, 2018, pp. 108–115
doi: 10.1093/jrr/rrx068
Advance Access Publication: 13 December 2017

Circular dichroism spectroscopic study on structural alterations of histones induced by post-translational modifications in DNA damage responses: lysine-9 methylation of H3

Yudai Izumi[1,*], Koichi Matsuo[1], Kentaro Fujii[2,3], Akinari Yokoya[2,3], Masaki Taniguchi[1] and Hirofumi Namatame[1]

[1]Hiroshima Synchrotron Radiation Center, Hiroshima University, 2-313 Kagamiyama, Higashi-Hiroshima, Hiroshima 739-0046, Japan
[2]Quantum Beam Science Directorate, National Institutes for Quantum and Radiological Science and Technology (QST), 2-4 Ooaza-Shirakata, Tokai, Naka, Ibaraki 319-1106, Japan
[3]QST Advanced Study Laboratory, National Institutes for Quantum and Radiological Science and Technology (QST), 2-4 Ooaza-Shirakata, Tokai, Naka, Ibaraki 319-1106, Japan
*Corresponding author. Hiroshima Synchrotron Radiation Center, Hiroshima University, 2-313 Kagamiyama, Higashi-Hiroshima, Hiroshima 739-0046, Japan. Tel: +81-82-424-6293; Fax: +81-82-424-6294; Email: izumi-yudai@hiroshima-u.ac.jp
(Received 15 August 2017; revised 13 October 2017; editorial decision 16 October 2017)

ABSTRACT

We report the global structural alterations in histone H3 proteins induced by lysine-9 mono-, di- and trimethylation, which are part of the critical post-translational modifications for DNA damage responses, identified using synchrotron radiation circular dichroism (CD) spectroscopy. Compared with unmodified H3, mono- and dimethylation increases the number of α-helices and decreases the numbers of β-strands, while trimethylation decreases the α-helix content and increases the β-strand content. Comparison of the secondary-structure contents of these histone H3 proteins suggests that the methylation-induced structural alterations occur at residues not only close to but also distant from the methylated sites. Such global structural alterations may regulate the interactions of methylated histones with other molecules, such as histone-binding proteins in DNA damage repair processes.

Keywords: post-translational modification; histone structural change; circular dichroism; synchrotron radiation

INTRODUCTION

A nucleosome comprises an octamer of four core histone proteins (H2A, H2B, H3 and H4) around which 146–147 base pairs of DNA are wrapped, and it is a basic building block of chromatin in eukaryotic nuclei [1, 2]. Post-translational modifications of histones, such as methylation, acetylation, phosphorylation and ubiquitination, have been shown to play substantial roles in cellular functions, such as DNA damage repair processes [3–8]. For example, lysine-9 (K9) trimethylated H3 (H3K9me3), which is produced via methylation of K9-monomethylated H3 (H3K9me1) [9], spreads over tens of kilobases away from DNA double-strand break (DSB) sites [10], and it is required for ATM-mediated DNA damage signaling [11]. Further, it is also known that K9 dimethylated H3 (H3K9me2) is required for BRCA1 and BARD1 retention at sites of DNA damage and associates with homologous recombination repair [12].

The mechanism of DNA repair processes via post-translational modifications other than H3K9 methylation has also been studied, as reviewed in detail elsewhere [8]. Generally, it is assumed that the dramatic alterations of chromatin structure that occur by post-translational histone modifications [5] make damaged sites more accessible for DNA repair proteins [13–15]. However, the structural changes in chromatin and histones induced by DNA damage responses (DDRs) *in vivo* are scarcely reported.

Recently, Izumi *et al.* investigated the secondary-structure contents of histones extracted from X-irradiated (40 Gy) and unirradiated HeLa cells using circular dichroism (CD) spectroscopy and

found the structural alterations of histones induced by DNA lesions: an increment of α-helix and a decrement of β-strand structures in H2A–H2B, and in contrast, a decrement of α-helix and an increment of β-strand ones in H3–H4 [16–18]. They hypothesized that post-translational modifications, such as the H3K9 methylation mentioned above, induced by DDRs alter the steric barrier and/or electrostatic interaction between modified residues and other residues; consequently, histone structures are changed. However, cellular histones are a difficult target for elucidating the structural alteration mechanisms by which they are modified because these include all post-translational modifications, such as methylation, acetylation, phosphorylation and ubiquitination, independently of the effects of artificial DNA lesions. Hence, to confirm the hypothesis, it is necessary to elucidate the structural alteration mechanism of histones induced by each modification related to DDRs from the bottom up.

Here, in an attempt to investigate the structural changes in H3 induced by K9 methylation, we measured the CD spectra of H3K9me1, H3K9me2, H3K9me3 and unmodified H3 (H3K9me0) recombinant proteins in the ultraviolet (UV) to vacuum-ultraviolet (VUV) region, which is a wavelength region shorter than about 200 nm, using a synchrotron radiation CD (SRCD) beamline.

CD is defined as the difference between the molar absorption coefficient for left circularly polarized light (LCPL) and that for right circularly polarized light (RCPL). CD spectra show susceptibility to the secondary structures of proteins, namely, α-helix, β-strand, turn and unordered structures. The structural information obtained from CD spectra is limited in the secondary structural level compared with that obtained by X-ray crystallography and nuclear magnetic resonance (NMR), which provide atomic-level structures. Nevertheless, CD spectroscopy, especially when using SRCD beamlines [19], is a powerful tool because it can provide us with structural information about proteins more easily than X-ray crystallography and NMR, owing to some notable advantages over these experimental methods [19]. For example, samples can be easily prepared by dissolving proteins in a solvent; that is, crystallization and isotopic substitution are not required. In addition, the required amount of sample is smaller than that used in X-ray crystallography and NMR, and therefore, CD spectroscopy is suitable for measurements of scarce proteins, such as modified histones.

Here, using SRCD spectroscopy, we are able to report the first observation of global structural alterations in histone H3 proteins induced by K9 methylation.

MATERIALS AND METHODS

Sample preparation

Recombinant *Xenopus laevis* unmodified and K9 methylated H3 proteins (purity > 98%) were purchased from Merck Millipore (product number 14-411; Billerica, MA, USA) and Active Motif [product numbers 31211 (H3K9me1), 31212 (H3K9me2), and 31213 (H3K9me3); Carlsbad, CA, USA], respectively. These samples demonstrated a single band in sodium dodecyl sulfate polyacrylamide gel electrophoresis (SDS-PAGE) analyses (Fig. S1 in supplemental information); therefore, they were used without further purification. Each sample was dissolved in 25 mM sodium phosphate buffer supplemented with 250 mM sodium fluoride (pH 8.6 at 25°C). Sodium fluoride was added to decrease electrostatic interactions among proteins and diminish the aggregation of H3 during measurements, because it is known that H3 slowly aggregates in sodium phosphate buffer [20]. The final concentration of each histone protein was 65 μM (1 mg/ml).

In this work, methylated H3 proteins whose K9 residues were replaced by aminoethylcysteine residues were used to have precise control over the site and degree of methylation [21]. Aminoethylcysteine is chemically and structurally similar to lysine [22]. Hence, histones containing methylated aminoethylcysteine are often used as an alternative for lysine-methylated histones to study, for example, the effect of methylation on nucleosome and chromatin structure [23] and the binding affinities between lysine-methylated histones and various histone-binding proteins [24]. Further, Timms *et al.* reported that the CD spectrum of *N*-acetylneuraminic acid lyase in which lysine-165 is replaced by aminoethylcysteine corresponds to that of wild type [25], showing that the effect of substitution is negligible for CD spectroscopy.

CD spectroscopy

CD spectroscopy was carried out at the BL12 beamline at the Hiroshima Synchrotron Radiation Center (HiSOR) in Japan [26]. The sample solution was encapsulated in a calcium fluoride (CaF_2) sample cell [27]. The path length of the CaF_2 cell was 12 μm. The samples were kept at 25°C. CD spectra were measured between 180 and 260 nm. The CD spectrum of the solvent, which should be zero under ideal conditions, was also measured as a baseline. We subtracted this baseline from the CD spectra of the samples to remove artificial CD signals that might have originated from the optical system, CaF_2 cells, and others.

The CD spectra with subtracted baseline were converted to molar CD ($\Delta\varepsilon$) to analyze the contents of the secondary structures. Molar CD is defined as

$$\Delta\varepsilon = \frac{\theta}{32980\ C\ N\ L}, \tag{1}$$

where θ, C, N and L are the CD intensity after subtraction of the baseline described as ellipticity (in millidegrees; obtained as raw data using the measurement system of the HiSOR BL12), the mol concentration of the sample, the number of amino acid residues of the samples, and the path length (in centimeters), respectively. Ellipticity θ is one of the expression methods of CD intensities used frequently and is proportional to the subtraction difference between absorbance for LCPL and that for RCPL.

Analysis of secondary structure

The contents of α-helix, β-strand, turn, and unordered structures in unmethylated/methylated H3 proteins were analyzed using CD spectra and the SELCON3 program [28, 29] based on reference data measured at HiSOR [30, 31]. We note that the α-helix content includes the 3_{10}-helix structure, and the content of unordered structures includes bend, π-helix and β-bridge structures. The numbers of α-helices and β-strands were calculated using the distorted contents of α-helix and β-strand structures [29]. The SELCON3 program was applied over the wavelength range of 185–260 nm.

Prediction of the positions of α-helices and β-strands

We predicted the positions of the α-helices and β-strands in unmethylated/methylated H3 proteins using a neural network (NN) method based on the CD spectroscopic results, which is termed the VUVCD–NN combination method [32], during which we regarded the methylated aminoethylcysteine residues in our samples as normal lysine residues. The computational protocol is described elsewhere [32]. Briefly, we used an NN algorithm [33] that predicts the positions of secondary structures using evolutionary sequence information based on the position-specific scoring matrices generated by the PSI-BLAST algorithm, under the limits of the number of α-helices and β-strands, and the number of amino acid residues composing α-helix and β-strand structures determined by CD spectroscopy and SELCON3 analyses. Turn and unordered structures estimated by SELCON3 analysis were classified as coil structures. It is known that the accuracy of the VUVCD–NN combination method is ~75% for 30 reference proteins [32].

Absorption spectroscopy

We compared the CD to absorption intensity ratio ($\Delta\varepsilon/\varepsilon$, where ε is the molar absorption coefficient), called the anisotropy factor or *g*-factor, of unmethylated/methylated H3 with that of other proteins [34] to verify the validity of the CD-measurement conditions. A commercial spectrophotometer (V-630 Bio; JASCO corporation, Tokyo, Japan), of which the path length is 0.1 cm, was used. Absorption spectra were measured between 220 and 300 nm, since the data obtained using the spectrophotometer were less reliable in shorter wavelength region. Absorbance *A* was converted to molar absorption coefficient comparing with the ratio of absorbance ($A_{275.5}$) to molar absorption coefficient at 275.5 nm ($\varepsilon_{275.5} = 4.04 \times 10^3\ M^{-1}\ cm^{-1}$ [35]): $\varepsilon/\varepsilon_{275.5} = A/A_{275.5}$.

RESULTS AND DISCUSSION

Absorption and CD spectra

Figure 1 shows the CD spectra of unmethylated/methylated H3 proteins. the absorption spectrum of H3K9me0 is also shown in Fig. 1. The absorption spectrum in the wavelength region longer than 260 nm is shown in the supplemental information (Fig. S2). Methylated H3 showed similar absorption spectra. The molar absorption coefficient increased toward the shorter wavelength region in Fig. 1. Since the anisotropy factors of unmethylated and methylated H3 in the 240–260 nm range were comparable with those of other proteins [34], we deemed our experimental conditions appropriate.

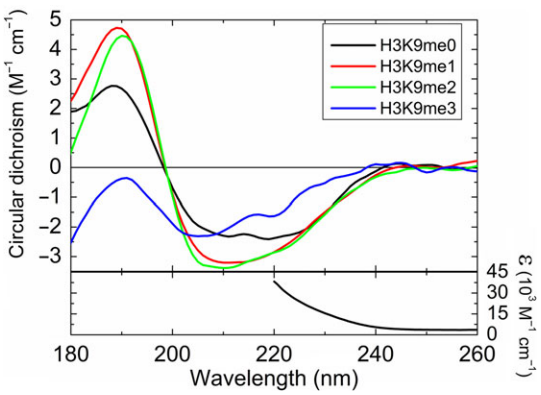

Fig. 1. (Upper panel) CD spectra of H3K9me0 (black), H3K9me1 (red), H3K9me2 (green) and H3K9me3 (blue). (Lower panel) Molar absorption coefficient (ε) of H3K9me0.

The CD spectrum for H3K9me0 exhibits a positive peak at ~190 nm and two negative peaks at ~210 and ~220 nm. These peaks are characteristic CD peaks of α-helix structures [36]. According to the pioneer study [20], the CD intensities at 220 nm of folded H3 in 25 mM sodium phosphate buffer without sodium fluoride were $-2.3\ M^{-1}\ cm^{-1}$ and gradually decreased to $-2.6\ M^{-1}\ cm^{-1}$ (24 h later) due to aggregation. As shown in Fig. 1, the CD intensity of H3K9me0 at 220 nm was $-2.3\ M^{-1}\ cm^{-1}$, and the intensity remained unchanged until the end of a series of H3K9me0-measurements (10 h after dissolving). Thus, aggregation of H3K9me0 was negligible in our conditions. Similarly, because the CD intensities of methylated H3 also remained unchanged, aggregation of methylated H3 was also negligible in our experiments, probably due to decreased interactions between histones and/or the increased stability of histones caused by adding sodium fluoride.

H3K9me1 exhibited CD peak positions similar to those of H3K9me0, but their CD intensities were very different. H3K9me2 exhibited a CD spectrum similar to that of H3K9me1, but H3K9me3 had a spectral shape that was quite different from H3K9me0/1/2, showing negative peaks at ~200–220 nm and no positive peak at ~190 nm.

As CD spectra reflect the contents of the secondary structures of proteins, these results show that methylation of K9 induces structural alterations in H3 proteins.

Secondary-structure contents

The CD spectra were analyzed using the SELCON3 program. The secondary structure contents of unmethylated and methylated H3 proteins, determined as the average of results obtained by SELCON3 program, are listed in Table 1, together with the standard deviations. The segment numbers of α-helices and β-strands are also listed in Table 1. For ease of comparison, the results in Table 1 are shown as in the proportional histograms of the secondary-structure contents seen in Figure 2, in which each secondary-structure content is normalized to a total content of 100%. The α-helix and β-strand structural contents in H3K9me0 were 24.4 ± 1.3% and 20.8 ± 1.6%, respectively, and the number of α-helices (N_α) and β-strands (N_β) were 4 and 6, respectively (Fig. 2 and Table 1). Turn and unordered structural contents in H3K9me0 were 20.6 ± 1.2% and 31.9 ± 1.6%, respectively.

H3K9me1 showed a large increment in the content and segment number of α-helix structures (24.4 ± 1.3% → 36.5 ± 1.7%; N_α = 4 → 6) and a decrement in those of β-strand structures (20.8 ± 1.6% → 13.6 ± 2.6%; N_β = 6 → 4), compared with those of H3K9me0 (Fig. 2 and Table 1). The contents of H3K9me2 were in agreement with those of H3K9me1 within the standard deviation (Fig. 2 and

Table 1. Contents of secondary structures of H3K9me0/1/2/3 obtained using the SELCON3 program

Structural content (%)	H3K9me0	H3K9me1	H3K9me2	H3K9me3
α-Helix	24.4 ± 1.3	36.5 ± 1.7	36.7 ± 1.5	13.1 ± 0.8
β-Strand	20.8 ± 1.6	13.6 ± 2.6	13.6 ± 2.4	29.6 ± 1.9
Turn	20.6 ± 1.2	23.1 ± 1.0	23.4 ± 1.6	22.7 ± 1.2
Unordered	31.9 ± 1.6	27.8 ± 1.8	27.4 ± 1.5	36.3 ± 2.4
No. of α-helices	4	6	6	3
No. of β-strands	6	4	4	8

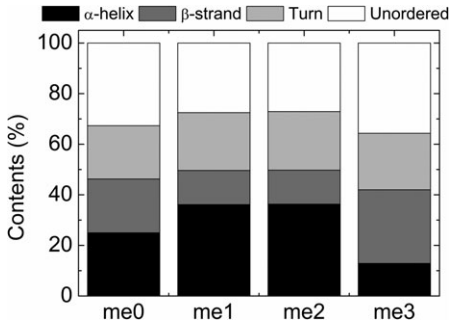

Fig. 2. Comparison of secondary-structure contents of H3K9me0 (me0), H3K9me1 (me1), H3K9me2 (me2) and H3K9me3 (me3) normalized to a total content of 100%.

Table 1). However, further methylation, namely, trimethylation of K9 in H3 (H3K9me3), induced a significant decrement in α-helix content (36.7 ± 1.5% → 13.1 ± 0.8%; $N_\alpha = 6 \rightarrow 3$) and an increment in β-strand content (13.6 ± 2.4% → 29.6 ± 1.9%; $N_\beta = 4 \rightarrow 8$) compared with those of H3K9me1 and H3K9me2 (Fig. 2 and Table 1). The content of turn structures scarcely changed through K9 methylations (Fig. 2 and Table 1). The contents of unordered structures were slightly decreased by K9 mono- and dimethylations, but increased by trimethylation (Fig. 2 and Table 1). These results suggest that structural alterations from unordered to α-helix and/or β-strand structures or their reverse changes, as well as those from α-helices to β-strands or *vice versa*, were induced by K9 methylation.

The content of α-helix structures largely varied by adding methyl group(s) (Fig. 2 and Table 1). In particular, comparing H3K9me1 or H3K9me2 with H3K9me3, the α-helix content varied by ~23.4%, which corresponds to structural changes in ~32 out of the 135 amino acid residues. Similar structural changes by methylations were also observed in β-strands. The significant structural alterations observed here could not be explained by alterations in only the residues neighboring the methylation site, implying that the K9 methylation-induced structural alterations were not just localized around the methylation site.

The predicted positions of α-helices and β-strands

Figure 3 shows predicted secondary-structure sequences of K9 unmethylated/methylated H3. Since the predictions of H3K9me1 and H3K9me2 showed the same results, these were shown together in Fig. 3 as 'me1/2'. In the case of H3K9me0, the structures from the first to the 44th residue, which include the N-terminal tail region, were assigned as coil, namely, turn or unordered structures. H3K9me1 and H3K9me2 formed a β-strand (or extended) structure from the fifth to the eighth residues in the simulation (Fig. 3). In the case of H3K9me3, this structure was also assigned. This shows that the additional methylations, namely di- and trimethylations, do not change the structures close to the methylation site. Because β-strand structures tend to form hydrogen bonds with neighboring atoms, the β-strand formations around the methylation site may contribute to the interaction with histone-binding proteins.

As shown in Fig. 3, the structural alterations are not limited to the region around the methylation site. For example, structural changes from β-strand to α-helix structures occurred at the 72nd–75th, 99th–100th and 128th–129th residues in the H3K9me1/me2 simulation. In H3K9me3, where many parts of α-helix structures observed in H3K9me1 and H3K9me2 changed to coil structures, some parts of the coil structures changed to β-strand structures. It is reported that methylation of cycloviolacin O2 [37] and phosphorylation of nitrogen regulatory protein C [38] and 2-oxoglutarate dehydrogenase multienzyme complex inhibitor (OdhI) [39] induce similar structural changes (coil to α-helix and β-strand structures, or their reverse changes) at residues distant from the modification site, using X-ray crystallography and NMR. These reports support our simulation, which predicted the structural alterations in the residues at locations distant from the methylation site. These structural changes would originate from changes to steric barriers and/or electrostatic interactions induced by methylation and from β-strand formation around the methylation site. Thus, our simulations based on CD spectroscopic results predicted that K9 methylation induces structural alterations of isolated H3 at residues not only adjacent to the methylated site but also distant from it.

Possible structural alteration mechanism induced by H3K9 methylation in solution

The methylation site in this study is located at the N-terminal tail of H3. It is known that the N-terminal tail forms unordered structures

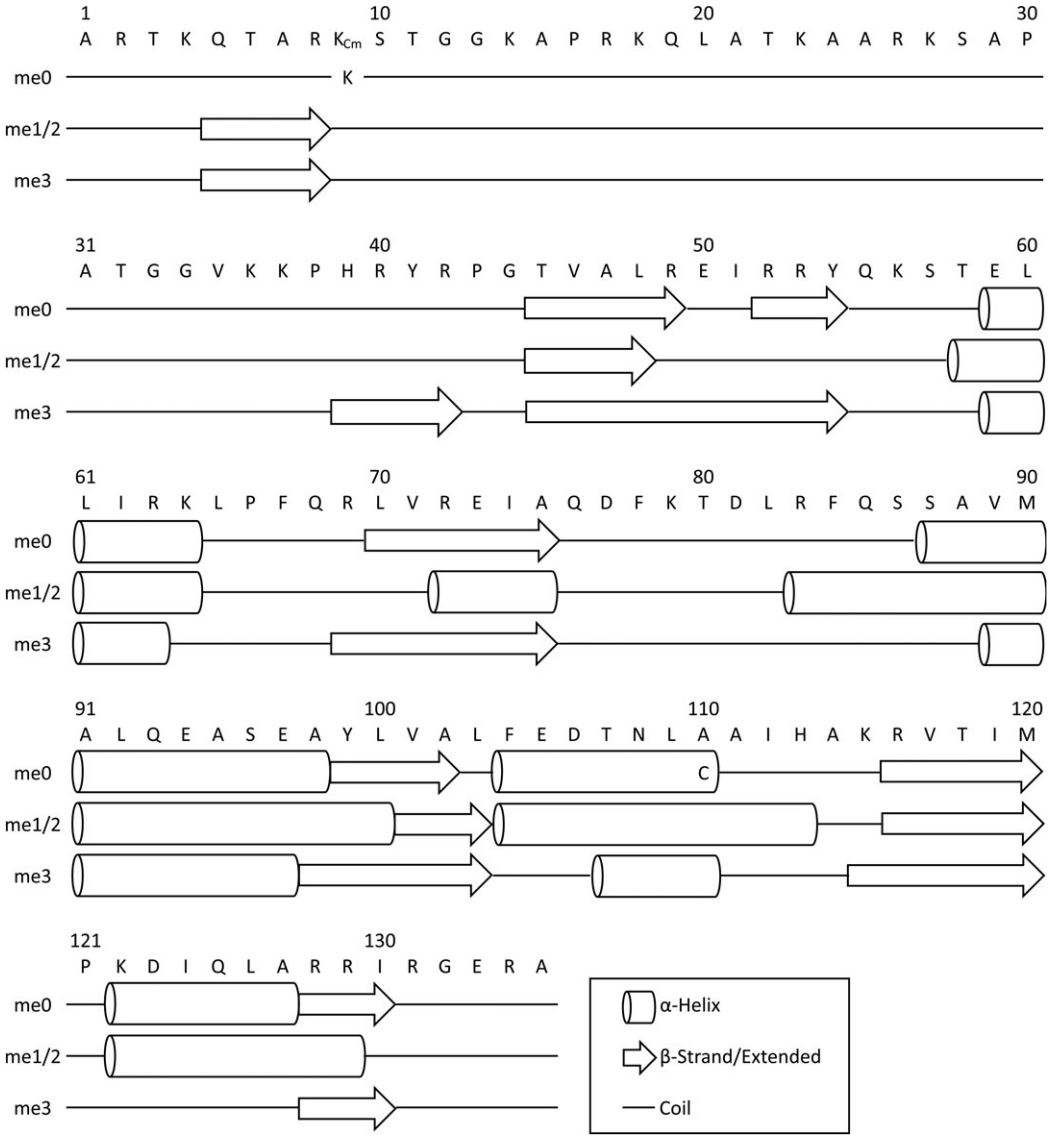

Fig. 3. Sequence-based secondary structures of H3K9me0 (me0), H3K9me1 and H3K9me2 (me1/2), and H3K9me3 (me3) obtained by the VUVCD–NN combination method. The α-helix, β-strand/extended, and coil structures are shown by cylinders, arrows and lines, respectively. The symbol K_{Cm} in the sequence represents methylated aminoethylcysteine inserted instead of methylated lysine (see Materials and Methods for details). Note that the 9th and 110th residues of H3K9me0 are lysine (K) and cysteine (C), respectively, which are different from those of methylated H3 samples.

in nucleosomal H3 and is isolated from the DNA and other core histones [2]. Hence, we could assume that all or most residues of the N-terminal tail of H3K9me0 also form unordered structures. This assumption was supported by our theoretical simulation, which predicted that the 1st–44th residues formed neither an α-helix nor a β-strand structure (Fig. 3). We observed an increment of the α-helices of H3K9me0 (~12.1%) and a decrease in the unordered structures (~4.1%) due to K9 mono and dimethylation; hence, these structural alterations scarcely occur only within the N-terminal tail when the balance of content change of α-helix and unordered structures is considered (Table 1). Therefore, it is expected that the structural alterations induced by K9 methylation should also occur in domain(s), of which secondary structures are not unordered structures, excluding an N-terminal tail. In this section, we propose a possible mechanism based on CD spectroscopic results and theoretical simulation. The simulation predicted that the structural alterations from β-strands to α-helices or their reverse changes mainly occurred at around the 40th–90th residues (Fig. 3).

A schematic view of the proposed mechanism for the structural alterations is shown in Fig. 4. In the unmodified state, the N-terminal tail would not interact with the other domain, as observed in nucleosomal H3 (Fig. 4a). K9 monomethylation would induce

changes in the steric barriers and/or electrostatic interactions around the methylation site, which might be the driving force of the secondary-structure formation(s) in the N-terminal tail. Dimethylation would induce similar changes. The structural changes following the methylation would also induce interaction of the N-terminal tail with residues distant from the methylation site (Fig. 4b). Through the interaction, those residues, referred to as M_1 residues hereafter, would form α-helix structure(s) (Fig. 4c). Indeed, similar dramatic structural changes were observed in the case of phosphorylation: phosphorylation induces folding of the unordered region of OdhI, and as a result, the phosphorylated part binds to its own FHA domain, and an α-helix is formed at residues distant from the phosphorylation site [39]. When the K9 is additionally methylated, the K9-trimethylated N-terminal tail would step away from the M_1 residues owing to changes in the steric barriers and electrostatic interactions, and then the structures of M_1 residues would revert to normal (α-helices → β-strands) (Fig. 4d). The K9-trimethylated N-terminal tail would interact with residues other than M_1 residues and trigger the structural alteration from α-helices to β-strands (Fig. 4e).

Apart from DDRs, H3K9 methylation plays other important roles. For example, H3K9me2 is associated with euchromatic gene silencing [40], and H3K9me3 is associated with heterochromatin condensation and epigenetic silencing in diverse organisms [41–45]. In *Caenorhabditis elegans*, H3K9me2 is required for activating the mitochondrial stress response [46]. To confirm the structural alteration mechanism induced by K9 methylation, more precise theoretical simulations, such as molecular dynamics (MD) simulations, are important and will be an interesting subject of future work.

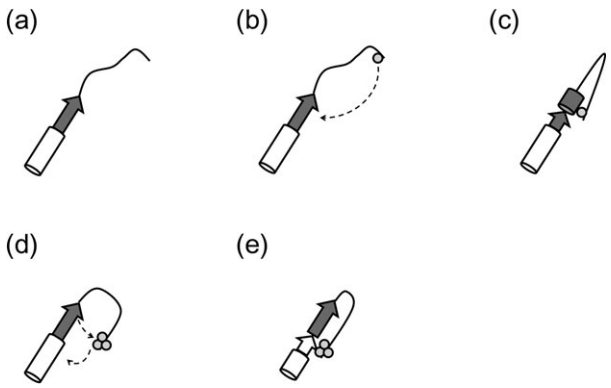

Fig. 4. Schematic view of the proposed structural alteration mechanism. The N-terminal tail region, which forms an unordered structure, is shown as curved lines. Cylinders, arrows and circles represent α-helices, β-strands and methyl groups, respectively. Secondary structures formed by M_1 residues (for details, see *Possible structural alteration mechanism induced by H3K9 methylation in solution*) are shown in gray and the others are shown in white. Turn structures are omitted. (a) A model of H3K9me0. (b) Monomethylated H3 before structural alteration. (c) The methylated N-terminal tail interacts with M_1 residues and as a result, induces structural changes from β-strands to α-helices. (d) The trimethylated N-terminal tail steps away from the M_1 residues, after which the structure of the M_1 residues would revert to normal (α-helices → β-strands). (e) The N-terminal tail interacts with domain(s) other than M_1 residues and induces structural changes from α-helices to β-strands.

Comparison of K9 methylated H3 with H3–H4 extracted from DNA-damaged cells

Izumi *et al.* irradiated human cancer cells with 40 Gy X-rays, and after that extracted H3–H4 [18]. H3K9me3 would spread over in total tens of megabases in 40 Gy X-irradiated cells because X-ray irradiation with 40 Gy induces ~1600 DSBs per cell [47] and H3K9me3 spreads tens of kilobases away from the DSB sites [10]. Nevertheless, the amount of H3K9me3 spreading tens of megabases would be only a few percent of the normal H3 because the human genome is ~3 gigabases. Therefore, the contribution of H3K9me3 to the secondary-structure contents of H3–H4 extracted from DNA-damaged cells would not be very large, and structural alterations observed in H3–H4 cannot be explained solely by trimethylation of H3 on K9, although the tendencies of the structural alterations are in agreement [18]. It is concluded that structural alterations of H3 induced by K9 trimethylation should be included during DDRs, but other post-translational modifications of H3, as well as H4, would also be required to explain the structural alterations of H3–H4 extracted from DNA-damaged cells.

Similar studies should be carried out in the future to confirm the structural alterations induced by other post-translational modifications during DDRs in both H3 and H4, such as methylations of lysine-79 on H3 and lysine-20 on H4, which link with the localization of 53BP1 around damaged DNA [8]. In addition, intermolecular interaction between H3 and H4 may also induce extra structural alterations. Other important future work will be to confirm structural alterations induced by post-translational modifications, under the coexistence of H3 and H4.

CONCLUSIONS

We have shown for the first time, using SRCD spectroscopy, that methylation of H3 on K9 induces global structural alterations, and we suggest that the alterations occur in residues not only adjacent to but also distant from the methylated site. The structural alterations would play important roles in DDRs. Cyclopedic CD spectroscopy of other modified histones will be an important part of future work aimed at understanding DNA damage repair processes.

The global structural alterations induced by K9 methylation would regulate the interactions between modified histones and other molecules, such as histone-binding proteins. The epigenetic functions of methylated H3 proteins *in vivo* may depend on structures not only in the vicinity of the methylation site but also distant from the site.

ACKNOWLEDGEMENTS

CD spectroscopy was carried out with the approval of the Hiroshima Synchrotron Radiation Center of Hiroshima University

(proposal numbers: 15A48 and 16AU007). The authors thank to Mr. Satoshi Yamamoto (Ibaraki University) for his experimental support.

CONFLICT OF INTEREST

The authors have no conflicts of interest to declare.

SUPPLEMENTARY DATA

Supplementary data are available at the *Journal of Radiation Research* online.

FUNDING

This work was supported by JSPS KAKENHI Grant Numbers JP15K16130 and JP17K12825.

REFERENCES

1. Luger K, Mäder AW, Richmond RK et al. Crystal structure of the nucleosome core particle at 2.8 Å resolution. *Nature* 1997; 389:251–60.
2. Davey CA, Sargent DF, Luger K et al. Solvent mediated interactions in the structure of the nucleosome core particle at 1.9 Å resolution. *J Mol Biol* 2002;319:1097–113.
3. van Attikum H, Gasser SM. Crosstalk between histone modifications during the DNA damage response. *Trends Cell Biol* 2009;19:207–17.
4. Pandita TK, Richardson C. Chromatin remodeling finds its place in the DNA double-strand break response. *Nucleic Acids Res* 2009;37:1363–77.
5. Hunt CR, Ramnarain D, Horikoshi N et al. Histone modifications and DNA double-strand break repair after exposure to ionizing radiations. *Radiat Res* 2013;179:383–92.
6. Price BD, D'Andrea AD. Chromatin remodeling at DNA double-strand breaks. *Cell* 2013;152:1344–54.
7. Gong F, Miller KM. Mammalian DNA repair: HATs and HDACs make their mark through histone acetylation. *Mutat Res* 2013;750:23–30.
8. Cao LL, Shen C, Zhu WG. Histone modifications in DNA damage response. *Sci China Life Sci* 2016;59:257–70.
9. Pinheiro I, Margueron R, Shukeir N, et al. Prdm3 and Prdm16 are H3K9me1 methyltransferases required for mammalian heterochromatin integrity. *Cell* 2012;150:948–60.
10. Ayraoetov MK, Gursoy-Yuzugullu O, Xu C et al. DNA double-strand breaks promote methylation of histone H3 on lysine 9 and transient formation of repressive chromatin. *Proc Natl Acad Sci U S A* 2014;111:9169–74.
11. Sasaki T, Lynch KL, Mueller CV et al. Heterochromatin controls γH2A localization in *Neurospora crassa*. *Eukaryot Cell* 2014;13:990–1000.
12. Wu W, Nishikawa H, Fukuda T et al. Interaction of BARD1 and HP1 is required for BRCA1 retention at sites of DNA damage. *Cancer Res* 2015;75:1311–21.
13. Smerdon MJ. DNA repair and the role of chromatin structure. *Curr Opin Cell Biol* 1991;3:422–8.
14. Soria G, Polo SE, Almouzni G. Prime, repair, restore: the active role of chromatin in the DNA damage response. *Mol Cell* 2012; 46:722–34.
15. Polo SE. Reshaping chromatin after DNA damage: the choreography of histone proteins. *J Mol Biol* 2015;427:626–36.
16. Izumi Y, Yamamoto S, Fujii K et al. Secondary structure alterations of histones H2A and H2B in X-irradiated human cancer cells: altered histones persist in cells for at least 24 hours. *Radiat Res* 2015;184:554–8.
17. Izumi Y, Fujii K, Wien F et al. Structure change from β-strand and turn to α-helix in histone H2A-H2B induced by DNA damage response. *Biophys J* 2016;111:69–78.
18. Izumi Y, Fujii K, Yamamoto S et al. DNA damage response induces structural alterations in histone H3–H4. *J Radiat Res* 2017;58:59–65.
19. Miles AJ, Wallace BA. Synchrotron radiation circular dichroism spectroscopy of proteins and applications in structural and functional genomics. *Chem Soc Rev* 2006;35:39–51.
20. D'Anna JA Jr, Isenberg I. Conformational changes of histone ARE (F3, III). *Biochemistry* 1974;13:4987–92.
21. Simon MD, Chu F, Racki LR et al. The site-specific installation of methyl-lysine analogs into recombinant histones. *Cell* 2007; 128:1003–12.
22. Gloss LM, Kirsch JF. Decreasing the basicity of the active site base, Lys-258 of *Escherichia coli* aspartate aminotransferase by replacement with gamma-thialysine. *Biochemistry* 1995;34:3990–8.
23. Lu X, Simon MD, Chodaparambil JV et al. The effect of H3K79 dimethylation and H4K20 trimethylation on nucleosome and chromatin structure. *Nat Struct Mol Biol* 2008;15:1122–4.
24. Voigt P, Reinberg D. Histone tails: ideal motifs for probing epigenetics through chemical biology approaches. *ChemBioChem* 2011;12:236–52.
25. Timms N, Windle CL, Polyakova A et al. Structural insights into the recovery of aldolase activity in *N*-acetylneuraminic acid lyase by replacement of the catalytically active lysine with γ-thialysine by using a chemical mutagenesis strategy. *ChemBioChem* 2013;14:474–81.
26. Sawada M, Namatame H, Taniguchi M. Optical design of a compact and practical UV beamline at HiSOR-BL12. *J Phys Conf Ser* 2010;425:162010.
27. Matsuo K, Sakai K, Matsushima Y et al. Optical cell with a temperature-control unit for a vacuum-ultraviolet circular dichroism spectrophotometer. *Anal Sci* 2003;19:129–32.
28. Sreerama N, Venyaminov SY, Woody RW. Estimation of the number of α-helical and β-strand segments in proteins using circular dichroism spectroscopy. *Protein Sci* 1999;8:370–80.
29. Sreerama N, Woody RW. Estimation of protein secondary structure from circular dichroism spectra: comparison of CONTIN, SELCON, and CDSSTR methods with an expanded reference set. *Anal Biochem* 2000;287:252–60.
30. Matsuo K, Yonehara R, Gekko K. Secondary-structure analysis of proteins by vacuum-ultraviolet circular dichroism spectroscopy. *J Biochem* 2004;135:405–11.
31. Matsuo K, Yonehara R, Gekko K. Improved estimation of the secondary structures of proteins by vacuum-ultraviolet circular dichroism spectroscopy. *J Biochem* 2005;138:79–88.

32. Matsuo K, Watanabe H, Gekko K. Improved sequence-based prediction of protein secondary structures by combining vacuum-ultraviolet circular dichroism spectroscopy with Neural Network. *Proteins* 2008;73:104–12.
33. Jones DT. Protein secondary structure prediction based on position-specific scoring matrices. *J Mol Biol* 1999;292:195–202.
34. McPhie P. Circular dichroism studies on proteins in films and in solution: estimation of secondary structure by *g*-factor analysis. *Anal Biochem* 2001;293:109–19.
35. D'Anna JA Jr, Isenberg I. A histone cross-complexing pattern. *Biochemistry* 1974;13:4992–7.
36. Greenfield N, Fasman GD. Computed circular dichroism spectra for the evaluation of protein conformation. *Biochemistry* 1969;8:4108–16.
37. Göransson U, Hermann A, Burman R et al. The conserved Glu in the cyclotide cycloviolactin O2 has a key structural role. *ChemBioChem* 2009;10:2354–60.
38. Kern D,Volkman BF, Luginbühl P et al. Structure of transiently phosphorylated switch in bacterial signal transduction. *Nature* 1999;402:894–8.
39. Barthe P, Roumestand C, Canova MJ et al. Dynamic and structural characterization of a bacterial FHA protein reveals a new autoinhibition mechanism. *Structure* 2009;17:568–78.
40. Tachibana M, Sugimoto K, Nozaki M et al. G9a histone methyltransferase plays a dominant role in euchromatic histone H3 lysine 9 methylation and is essential for early embryogenesis. *Genes Dev* 2002;16:1779–91.
41. Bannister AJ, Zegerman P, Partridge JF et al. Selective recognition of methylated lysine 9 on histone H3 by the HP1 chromo domain. *Nature* 2001;410:120–4.
42. Lachner M, O'Carroll D, Rea S et al. Methylation of histone H3 lysine 9 creates a binding site for HP1 proteins. *Nature* 2001; 410:116–20.
43. Nakayama J, Rice JC, Strahl BD et al. Role of histone H3 lysine 9 methylation in epigenetic control of heterochromatin assembly. *Science* 2001;292:110–3.
44. Jacobs SA, Taverna SD, Zhang Y et al. Specificity of the HP1 chromo domain for the methylated N-terminus of histone H3. *EMBO J* 2001;20:5232–41.
45. Nielsen SJ, Schneider R, Bauer UM et al. Rb targets histone H3 methylation and HP1 to promoters. *Nature* 2001;412:561–5.
46. Tian Y, Garcia G, Bian Q et al. Mitochondrial stress induces chromatin reorganization to promote longevity and UPR^{mt}. *Cell* 2016;165:1197–208.
47. von Sonntag C. *Free-radical-induced DNA Damage and its Repair*. Berlin/Heidelberg: Springer, 2006.